Article:
Tang, T-C, Amadei, CA, Thomson, NH et al. (1 more author) (2014) Ion exchange and DNA molecular dip sticks: studying the nanoscale surface wetting of muscovite mica. Journal of Physical Chemistry C, 118 (9). 4695 - 4701. ISSN 1932-7447

https://doi.org/10.1021/jp411125n

Ion-Exchange and DNA Molecular Dip-Sticks: Studying the Nnanoscale Surface Wetting of Muscovite Mica

Tzu-Chieh Tang,[1] Carlo A. Amadei,[1] Neil H. Thomson,[2,3] Matteo Chiesa[1*]

[1] Laboratory for Energy and NanoScience (LENS), Institute Center for Future Energy (iFES), Masdar Institute of Science and Technology, Abu Dhabi, UAE

[2] Molecular and Nanoscale Physics Group, School of Physics and Astronomy, University of Leeds, LS2 9JT, UK

[3] Department of Oral Biology, School of Dentistry, University of Leeds, LS2 9LU, UK

[*] Corresponding author, email:: -mchiesa@masdar.ac.ae, telephone number: +971 2 810 9333

ABSTRACT

Mica is an abundant crystal mineral that has important and interesting bulk and surface properties for a variety of applications. These arise from its anisotropic structure where layers of aluminium silicate, 1 nm thick, are ionically bonded together, typically with K^+ ions. The surface properties of mica can be varied through ion-exchange with the exposed lattice sites. In this study, the effect of kinetics on ion exchange with nickel ions (Ni^{2+}) and its influence on surface water thickness as a function of time has been investigated. Mica was ion-exchanged for 30 seconds or 5 minutes for a range of Ni^{2+} concentrations (i.e. 1.0 to 20.0 mM) and its surface properties measured for up to 96 hours after incubation in a controlled environment. The nanoscale physico-chemical properties of nickel-functionalized Muscovite mica (Ni-mica) were investigated by reconstructing the conservative force profile between an atomic force microscopy (AFM) tip and the surface. This gives a direct measure of the surface water thickness and enables details of the spatial and temporal variations in surface properties due to the ion mediated adsorption of water to be elucidated. Variations in the water layer thickness were confirmed by using non-contact AFM imaging in ambient and DNA molecules as "molecular dip-sticks". It was found that the surface properties were largely independent of the incubating concentration but did depend on the incubation time during ion exchange and the ageing time. For the longer incubation time of 5 minutes, the water layer thickness remained constant around ~1.5nm deep whereas for short incubation times of 30 seconds, the thickness was initially sub-nanometer but grew with ageing time and converged to a similar final value after 96 hours. The extracted force of adhesion (F_{AD}) also showed the same trends, where reduced values of F_{AD} indicated increased screening of the van der Waals interaction through thicker water layers.

KEYWORDS: Ion Exchange, Wetting, Adsorption, Nickel Chloride, AFM

INTRODUCTION

Muscovite Mica is an alumino-silicate mineral that due to its anisotropic layered structure, chemical stability and smooth surface has long had applications as a thermal and electrical insulator[1,2] but is finding increasing interest in basic and applied research. The cross plane structure of mica is made of 1 nm thick dioctahedral aluminum silicate layers ionically bonded together typically by potassium ions (K^+). When cleaved, the atomically smooth planar surface is exposed and terminated in oxygen atoms. The surface is characterized by a negative lattice charge due to the periodic replacement of the Si atoms by Al, but this resultant negative charge is exactly balanced by K^+ or Na^+ ions, where they are present from the original crystal. Cleaving a single plane of mica will leave half the ionic sites occupied and half unoccupied on the revealed surfaces[3]. Under ambient conditions, one might expect these empty sites to be replaced with ions via water-mediated processes, as mica is a very hydrophilic high energy surface that readily attracts water molecules.

In aqueous solution, these surface ions can be exchanged with other inorganic or organic cations[4] modifying the surface properties of the muscovite mica. Ion exchange is obtained by immersing the exposed surface in aqueous electrolyte solutions. This allows the ions on the mica surface[4] to be replaced with a wide range of other multivalent cations. Early investigations of the interaction between two cleaved mica surfaces immersed in various metal-ions solutions was carefully carried out with the aid of the surface force apparatus (SFA)[5,6,7]. The combination of the effect of the shorter range van der Waals attraction and the electrostatic repulsion due to the electrical double layer of counter-ions in the solution is well described in terms of the Derjaguin-Landau-Verwey-Overbeek (DLVO) theory. These SFA studies have been important in shedding light on

fundamental aspects of the ion exchange mechanism but do not give information on the local properties of these surfaces at the nanoscale[8]. Techniques based on dynamic atomic force microscopy (dAFM) enable the force profiles above surfaces to be probed[9] as well as non-contact imaging of water behavior and structure[10,11].

We consider mica ion-exchanged with nickel ions (Ni^{2+}) due to its importance in the study of biological samples by means of atomic force microscopy (AFM) in both liquid and air[12,13,14,15,16,17,18,19]. Interestingly the effect of kinetics on ion exchange with nickel ions (Ni^{2+}) and its influence on the adsorption of water from the atmosphere as a function of time is still scarcely understood.

The present study complements the existing body of knowledge by investigating the nanoscale physicochemical properties of nickel-functionalized Muscovite mica. Specifically we detect the effects that metal ions have on the water accumulation on the mica surface by means of amplitude modulated atomic force microscopy (AM AFM). First we employ a single double-stranded DNA molecules anchored on nickel-treated mica surfaces as a "molecular dip-stick" to corroborate the water layer thickness by means of non-contact AFM imaging in ambient. Our results confirm the role that water layers, forming on the tip and on the sample's surface, play in the capability of recovering the true height by means of AM-AFM experiments. Second we investigate the role that ion-exchange treatment has in modifying the physicochemical characteristics of the mica surfaces. By using the Sader[20]-Jarvis-Katan[21] formalism and in situ tip radius monitoring[22,23], we reconstruct experimentally the conservative force profile between tip and nickel-coated mica surface. For a thorough survey on the effects of surface treatment, five different Ni^{2+} concentrations (1.0, 2.5, 5.0, 10.0, and 20.0 mM) are applied and tested under two incubation times (30 sec and 5 min). Meanwhile, forces measured at four time points after ion deposition (12, 24, 48, and 96 hours) are

used to investigate the aging effect when samples are exposed in room humidity (~ 0.5). In order to quantify the conservative interactions, two parameters are introduced (ΔdF_{AD} and A_{AD}) which reveal how the ion concentration plays a minor role compared to the length of incubation and/or aging period. Moreover, the above parameters allow determining the accumulation of water layer[22-23]. Both parameters show a 1.5-2.0-fold increase when the samples are treated with Ni^{2+} solution for 5 minutes or left exposed in air for 4 days. These results suggest two important features of the ion exchange mechanism. First, the nickel ions attach to freshly cleaved mica surface in a time-dependent fashion, where longer incubation time allows more firmly adhesion events to occur. Second, the presence of ions on the mica surface modifies its adsorption isotherm and changes the amount of water molecules that can be attracted to the surface until thermodynamic equilibrium is reached (Figure 1)[24].

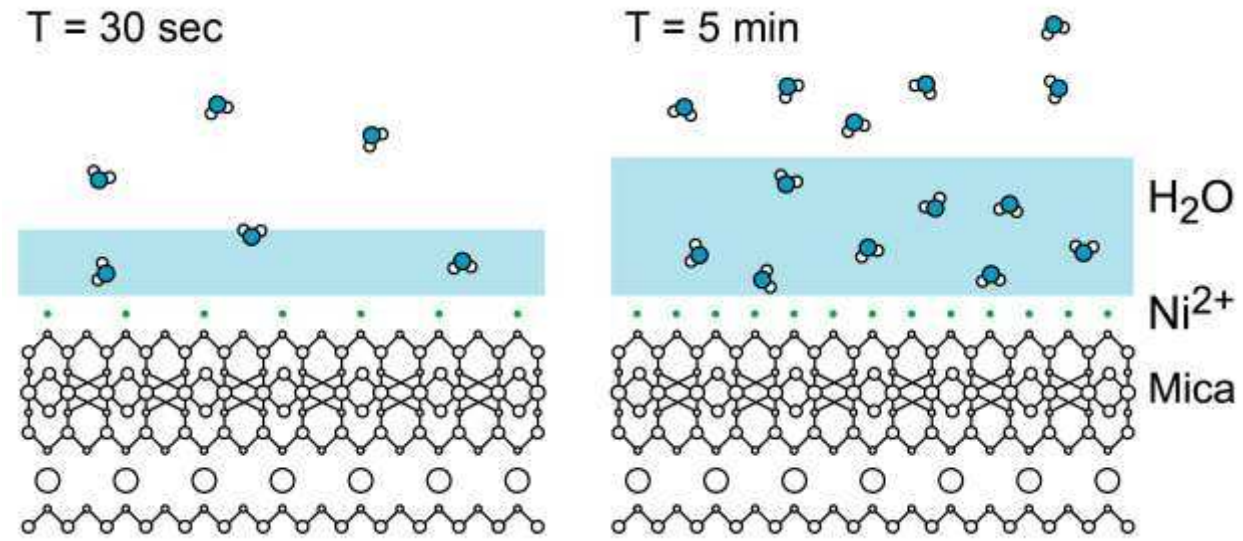

Figure 1: Scheme exemplifying the difference in water layer thickness between samples treated with nickel ion solution for 30 seconds and 5 minutes.

EXPERIMENTAL METHODS

Nickel Ion Deposition on Mica. $NiCl_2$ solutions were diluted into 1.0, 2.5, 5.0, 10.0, and 20.0 mM concentrations from 1M stock using Milli-Q water. Buffer solutions of 40mM of HEPES plus each concentration of $NiCl_2$ were adjusted to pH 6.8 using NaOH. Mica discs were cleaved immediately before using Scotch Magic tape. After cleavage, 50 µL aliquots of $NiCl_2$ buffer were applied onto the mica discs and left for a given incubation time of 30 sec or 5 min. Then, the discs were rinsed with Milli-Q water and blown dry using 99.9% pure N_2 gas. All samples were kept in a sealed sample container to avoid contaminants until time of measurement.

DNA Sample Preparation. PCR amplified linear DNA molecules (1025 bp) from YCp111 plasmid were cleaned up using QIAquick Gel Extraction Kit (QIAGEN) and dissolved in 5mM of $NiCl_2$ buffer to make a 5 µg/mL stock solution. Before experiment, the DNA solution was diluted with 5mM of $NiCl_2$ buffer to reach the final concentration of 1 µg/mL. Aliquots of 50 µL were applied on freshly cleaved mica discs and left to incubate for 30 seconds. The samples were then rinsed with Milli-Q water, blown dry by 99.9% N_2 gas, and kept in a sealed container until time of imaging.

AFM. All experiments on nickel treated samples were carried out using an Asylum Research Cypher Atomic Force Microscope. To minimize the effects of higher eigen-modes and approximate the motion to the first harmonic[25], the cantilever OLYMPUS AC160TS (spring constant (k) ≈ 40 N/m, quality factor (Q) ≈ 500, resonance frequency ($f = f_{0)} \approx$ 300 kHz and tip radius (R) ≈ 7 nm) is used in collecting all force curves in the dynamic mode. Images were acquired in non-contact (NC) AFM. During imaging, we operated at free amplitude of 4 nm and set-point of 3 nm. The resolution of images were 512 × 512 pixels over a 500 nm × 500 nm area and the scan rate was 0.5 Hz. The apparent height is measured as the distance between the apex of the

profile and the average height of the whole image which is defined as zero. The values presented in the text were the averages calculated from twenty profiles from each image.

Force Reconstruction. The force reconstruction exploits the Sader-Jarvis-Katan formalism[21] (Eq. (2)). In this formalism, the force F_{ts} versus minimum distance of approach d_m is recovered from variations in the frequency shift Ω that occurs by decreasing the cantilever-sample separation (z_c). The cantilever-surface separation z_c can relate d_m, or equivalently d, to the oscillation amplitude A:

$$d_{min} \equiv d \approx z_c - A \qquad (1)$$

Then, the normalized conservative force F_{ts}^* reads:

$$F_{ts}^*(d) = \frac{2k}{|F_{AD}|}\int_{u=d}^{u=\infty}\left[\left(1+\frac{A^{1/2}(u)}{8\sqrt{\pi(u-d)}}\right)\Omega(u) - \frac{A^{3/2}(u)}{\sqrt{2(u-d)}}\frac{d\Omega(u)}{du}\right]du \qquad (2)$$

For each curve, the normalization is carried out with the absolute value of the minimum of force (force of adhesion, F_{AD}) and where Ω is the normalized frequency shift expressed by:

$$\Omega(d) = \left[1+\frac{A_0}{QA}\cos(\Phi(d))\right]^{\frac{1}{2}} - 1 \qquad (3)$$

In Eq. (3), A_0 is the free amplitude of oscillation while Φ is the phase lag relative to the drive force. In order to recover the whole range of d, A_0 needs to be finely controlled. This allows a smooth transition from the attractive to the repulsive regime to be achieved, i.e. avoiding bi-stability and discontinuity in the amplitude-phase-distance (APD) curves[26,27]. For OLYMPUS AC160TS cantilevers and with $5 < R < 10$ nm, avoiding bi-stability requires $20 < A_0 < 30$ nm for Ni^{2+} coated mica samples. For the freshly prepared sample, it was not possible to achieve smooth transitions with relatively small free amplitude ($A_0 < 60$ nm). The tip radius R has been constantly monitored

in situ by using the A_C method, which measures the critical amplitude where the transition from the attractive to the repulsive regime occurs[28]. Moreover, peak forces can be tuned by carefully selecting the minimum reduction in amplitude (for example, 90% of A_0) in order to reduce sample invasiveness and area of interaction[23,10,29].

RESULTS AND DISCUSSION

NC AFM imaging: DNA Molecular Dip-Sticks Indicate Water Layer Thickness on Ni^{2+} Treated Mica Surface.

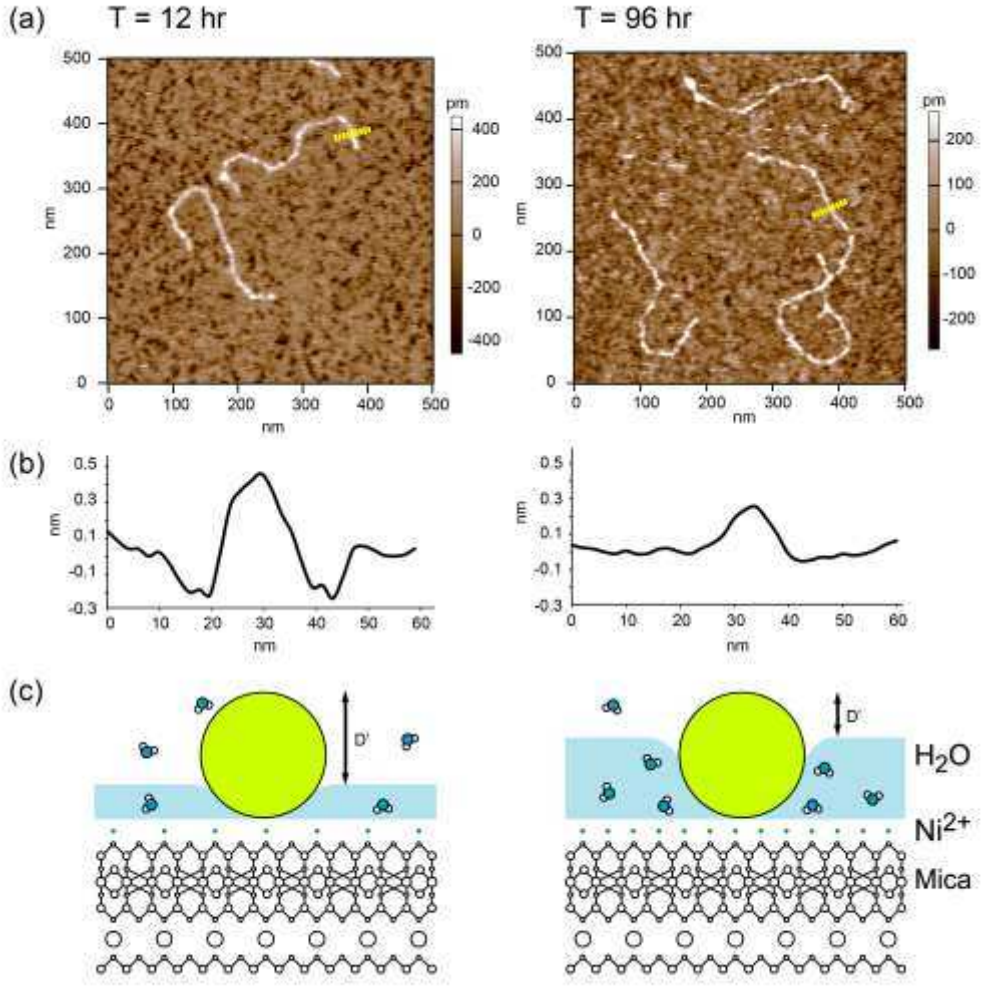

Figure 2: NC AFM images of DNA molecules (a) on mica surface treated with $NiCl_2$ solution for 30 seconds which undergoes aging processes of 12 hours and 96 hours. The cross-sections (b) show the apparent height profiles of DNA molecules at position indicated in yellow dash lines in (a). In (c), the scheme describing the change in apparent height (D') due to the difference in water layer thicknesses as a result of sample aging.

True non-contact imaging by dynamic AFM (NC AFM) can be achieved in ambient conditions with water layers present on both the tip and the sample[30]. Operating conditions can be found where neither of the water layers is disturbed because the change in the cantilever amplitude used to profile the surface arises from the long range van der Waals interaction. These conditions are met when the cantilever free amplitude $A_0 << 1/2A_c$ (the critical amplitude for bi-stability) as is the case for the imaging in this study.

The loss of apparent height of macromolecules has been debated strongly in the AFM community[31]. In addition to the intrinsic resolution limit causing height information, the role of adsorbed water on the substrate is recognize to play a role[32]. The AFM is operated in a Non-Contact imaging conditions in order to disregard the effects of sample deformation on the loss of height[30].

Without mechanical contact between tip and surface, the physical size and chemical state of the tip can be preserved allowing quantitative comparative measurements to be made between different samples using the same AFM probe. Moreover, recent methods to accurately size the AFM tip in situ and monitor any changes to its physical size[28] as well as defining the tip size through controllable wear at the nanoscale[33] enable quantitative comparison between samples using different AFM probes.

Figure 2a shows images taken on the same mica sample using the same AFM tip which has been treated for 30 seconds with Ni ions but aged for 12 and 96 hours. The size of the tip was tracked constantly by the A_c method throughout the experiment (the measured A_c is around 8 nm and tip radius ≈ 4 nm, according to Ref.18). The apparent heights of selected linear DNA molecules at each time point show that the water layer thickness increases with greater ageing time (Figure 2b). The diameter of a double-strand DNA is well-defined by its stable double helical structure and for B-form is 2 nm[34,35], making it an effective height calibration standard for the effects of water on the surface of the mica, i.e. a molecular dip-stick. The apparent height of nanoscale objects profiled by a similar sized tip are usually less than the real height, which is a consequence of the geometrical convolution of the force fields between the two objects[36]. This is also valid for NC AFM as can be seen in Figure 2 where the apparent height of the DNA is ~~~~0.8~~0.45 ± 0.04 nm at 12 hours ageing time but decreases to 0.23 ± 0.02 ~~~~0.3~~nm after 96 hours. Importantly, sample deformation is negligible since we were operating in NC mode at A/A_0 = 0.7-0.8[30].

Interestingly, the variation of the height profile of the 96 h image (≈ 500 pm) is relatively small compared to the 12 h image (≈ 1000 pm), as shown in the scale bar. This suggests that the surface is reaching thermodynamic equilibrium with the surroundings.

The AFM tip size was checked to remain the same between both images which leads to the conclusion that the water layer is deeper on the older sample (Fig. 2c).

This exemplifies the effect of the accumulation of water on the surface as the sample ages, and led us to test the water layer thicknesses on Ni-mica after two incubation times and different ageing times. This was directly measured in the AFM using a dynamic force spectroscopy approach where the force profile as a function of separation distance between tip and sample was reconstructed.

The vertical extent and integrated force associated with the tip interacting with the water layer give two metrics to characterize the water layer.

Force Reconstruction: Effects of Ni^{2+} Concentration and Aging on Surface Water Layers

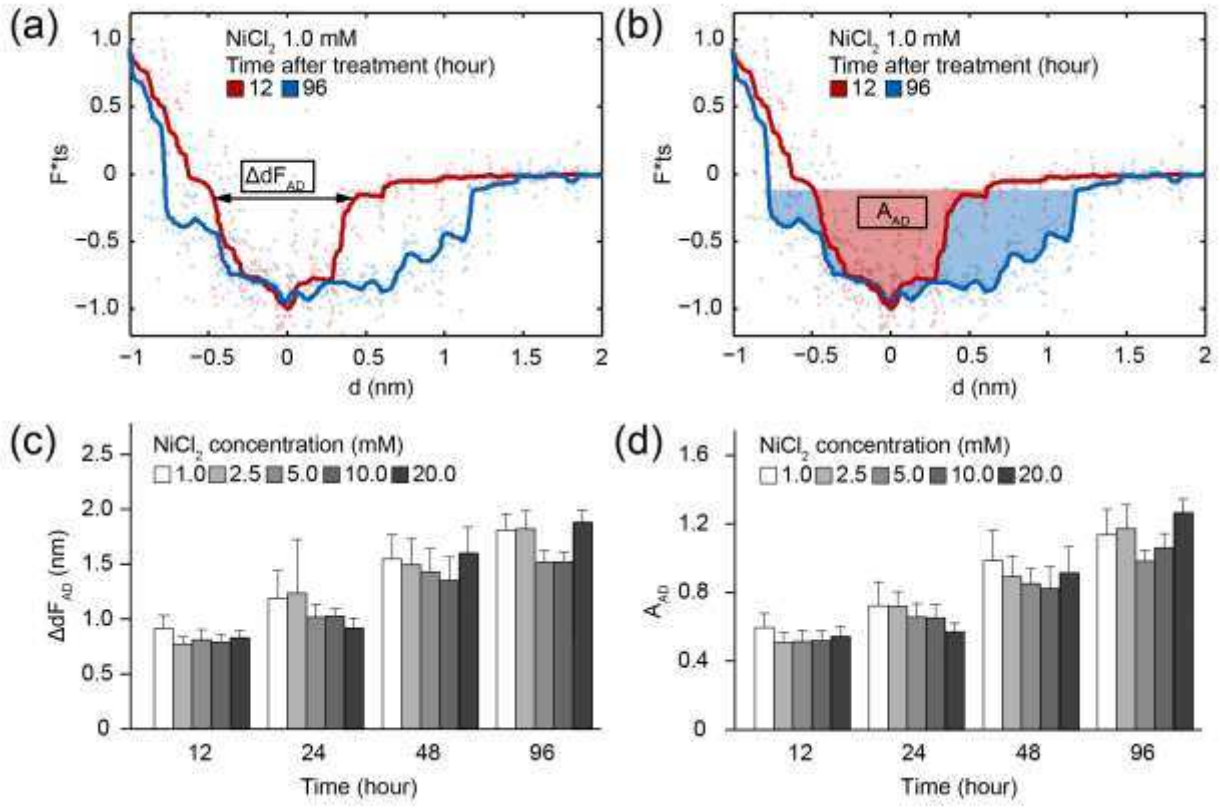

Figure 3: Normalized force profiles of mica surface incubated with 1.0 mM $NiCl_2$ solution for 30 seconds versus d. (a) shows the ΔdF_{AD} and (b) shows the A_{AD} at 12 hours (red) and 96 hours (blue) after ion-exchange treatment. The comparisons of ΔdF_{AD} and A_{AD} at different $NiCl_2$ concentrations are presented in (c) and (d), respectively. Each bar represents 15 force curves taken at different regions of the surface.

To understand the effects of ion concentration and aging process on tip-sample interaction, we incubated all samples for 30 seconds and performed 15 force measurements at each certain time point. Data acquired immediately after treatment are not included because of the instability of the

surface during the early stage of ion exchange. The force profiles were then recovered from the amplitude-phase-deflection (APD) randomly taken on the surface as explained above.

Two metrics are exploited in order to quantify the mica surface properties through these force curves. First, ΔdF_{AD} can be recovered from F_{ts}^* plotted against the tip-sample distance (d) as follows. We select a reference point ($d \approx 0$) coinciding with the distance at which the F_{ts}^* minimum is reached. Next, the distance between the two points where $F_{ts}^* = 0.2$ is measured and defined as ΔdF_{AD}. The cut-off value 0.2 is chosen because it is representatively sensitive for width measurement and yet not prone to the fluctuation and deviation of curve fitting. ΔdF_{AD} acts as an indicator of the width of the trough of the force profile (Fig. 3a). Similarly, the area defined by the force profile, under the threshold where $F_{ts}^* = 0.05$, is calculated as the shaded area under adhesion force (A_{AD}) in Fig. 3b. It is worth noting that by using A_{AD} we can bypass the arbitrarily selection of a cut-off value like in the calculation of ΔdF_{AD} and obtain more reliable results. From Figs. 3a and 3b, one can easily see that these two metrics demonstrate similar behaviours as the aging evolved from 12 h to 96 h. As suggested in our previous studies[22-23], the widening of the trough corresponds to the increase in the thickness of water layer adsorbed on the surface, thus ΔdF_{AD} and A_{AD} represent viable parameters to monitor the evolution of the adsorbed water film thickness. In Fig. 3c, the ΔdF_{AD} increases ~~linearly~~ from 12 h to 96 h (from 8.24 ± 0.48 Å to 17.07 ± 1.01 Å), which indicates the constant accumulation of water on the surface. As expected, the identical increase is observed in A_{AD} as shown in Fig. 3d. Note that the increase of the two values of the two parameters is determined by longer range van der Waals interactions (non-mechanical contact between the tip and the sample). In particular, in the 12 h curve the interaction starts at 0.5 nm above the surface while in the 96 h the distance of interaction doubles. The Ni^{2+} adsorbed on mica

modifies the adsorption isotherm of water on the surface and contributes to the attraction of water molecules from the surrounding environment as was observed by other groups[24].

Against expectation, when compared to the length of the aging process, the concentration of the $NiCl_2$ solution does not play such an important role in determining the accumulation of water on surface. Under all five concentrations tested, no significant variation can be observed in ΔdF_{AD} and A_{AD} within each time point as shown in Fig. 3c and Fig. 3d, respectively. For example, at the 12 h time point, the ΔdF_{AD} of the five concentrations are 9.16 ± 1.18 Å, 7.73 ± 0.67 Å, 8.12 ± 0.93 Å, 7.90 ± 0.67 Å, and 8.31 ± 0.65 Å for 1.0, 2.5, 5.0, 10.0, and 20.0 mM, respectively (For complete data, see Table 1). This observation suggests that the kinetics of binding of the Ni ions into available surface sites is equally efficient over the concentration range and implies that the resultant surfaces have a similar surface energy since their ability to attract water molecules from humid vapour is the same and leads to equal water layer thicknesses.

Table 1: ΔdF_{AD} Values under All Conditions Tested. Each number represents the average and standard error of 15 force curves.

	ΔdF_{AD} (Å)			
Time after deposition	**12 h**	**24 h**	**48 h**	**96 h**
$NiCl_2$ concentration	**Incubation time = 30 seconds**			
1.0 mM	9.16 ± 1.18	11.86 ± 2.55	15.48 ± 2.20	18.12 ± 1.46
2.5 mM	7.73 ± 0.67	12.27 ± 4.89	14.96 ± 2.34	18.21 ± 1.65
5.0 mM	8.12 ± 0.93	10.16 ± 1.14	14.29 ± 2.12	15.18 ± 1.08
10.0 mM	7.90 ± 0.67	10.26 ± 0.68	13.53 ± 2.13	15.20 ± 0.91
20.0 mM	8.31 ± 0.65	9.20 ± 0.88	15.99 ± 2.40	18.81 ± 1.08
	Incubation time = 5 minutes			
1.0 mM	14.39 ± 1.09	14.81 ± 0.72	13.95 ± 1.91	14.34 ± 2.06
2.5 mM	13.16 ± 0.85	13.85 ± 1.06	14.82 ± 1.70	17.05 ± 0.99
5.0 mM	12.53 ± 1.81	15.71 ± 1.87	16.33 ± 1.83	13.98 ± 1.08
10.0 mM	13.88 ± 0.41	13.23 ± 1.79	12.83 ± 0.87	15.40 ± 1.33
20.0 mM	13.33 ± 1.20	13.12 ± 0.95	14.42 ± 1.17	17.40 ± 1.17

Effects of Incubation Time. We further examined the importance of the length of incubation period by extending it from 30 seconds to 5 minutes and by recovering 15 force profiles for each time stage. The force profiles from this set of data (5 minute) exhibit similar behaviors as all curves share almost the same trough widths. Indeed, in Fig. 4a and Fig. 4b, the F_{ts}* profiles at 12 h and 96 h nicely overlap, implying similar tip-sample interactions. Likewise the ΔdF_{AD} (Fig. 4c) and A_{AD} (Fig. 4d) reach the maximum at 12 hours after deposition and remain at this level throughout the entire scope of observation. In particular, $\Delta dF_{AD} \approx 1.5$ nm and $A_{AD} \approx 0.8$. This implies that the water accumulation due to adsorption does not increase as the samples are exposed in air for a longer time. This is also demonstrated by the constant distance range of van der Waals long range interactions (i.e. $d \approx 1$ nm). Again, as observed for the 30 second incubation time, the nickel ion solution concentration during ion-exchange has negligible effects on the subsequent values of ΔdF_{AD} and A_{AD}. These results suggest that 5 minutes of incubation is

sufficient for nickel ions to attach onto all possible binding sites on mica and further that they stay firmly on the surface without being washed away in the rinsing step. Moreover, the amount of water adsorption of the 5 min incubation/12 h aging data point is comparable to the amount of the 30 sec incubation/96 h aging set, which means that the maximal water layer thickness can be reached within 12 hours by prolonging the Ni ion incubation time. This phenomenon can be also explained by means of normalized force of adhesion (F^*_{AD}) in Fig. 5, as they decrease to 40% and 60% of the value at 12 h for 30 sec and 5 min treatment, respectively. Comparing the ion-exchanging mica to the mica control, one observes a significant difference in reaching thermodynamic equilibrium with the vapour atmosphere. The untreated mica surface reached equilibrium within 12 hours, while the treated ones took at least 24 to 48 hours to reach stable states. The decrease in F_{AD} is a reflection of the accumulation of water that continues until thermodynamic equilibrium with the vapour atmosphere is reached. This growing water layer screens the van der Waals interaction between mica and tip resulting in a reduction in F_{AD} with time. Moreover, the F_{AD} in the 5 min incubation set remains relatively constant, in the range of 0.8-1.5 nN. However, the F_{AD} in the 30 sec group dropped drastically from 3 nN to near 1 nN. This agrees with the interpretation that the water layer thickness remains, for the 5 minute case, rather constant with time as presented in Fig. 4.

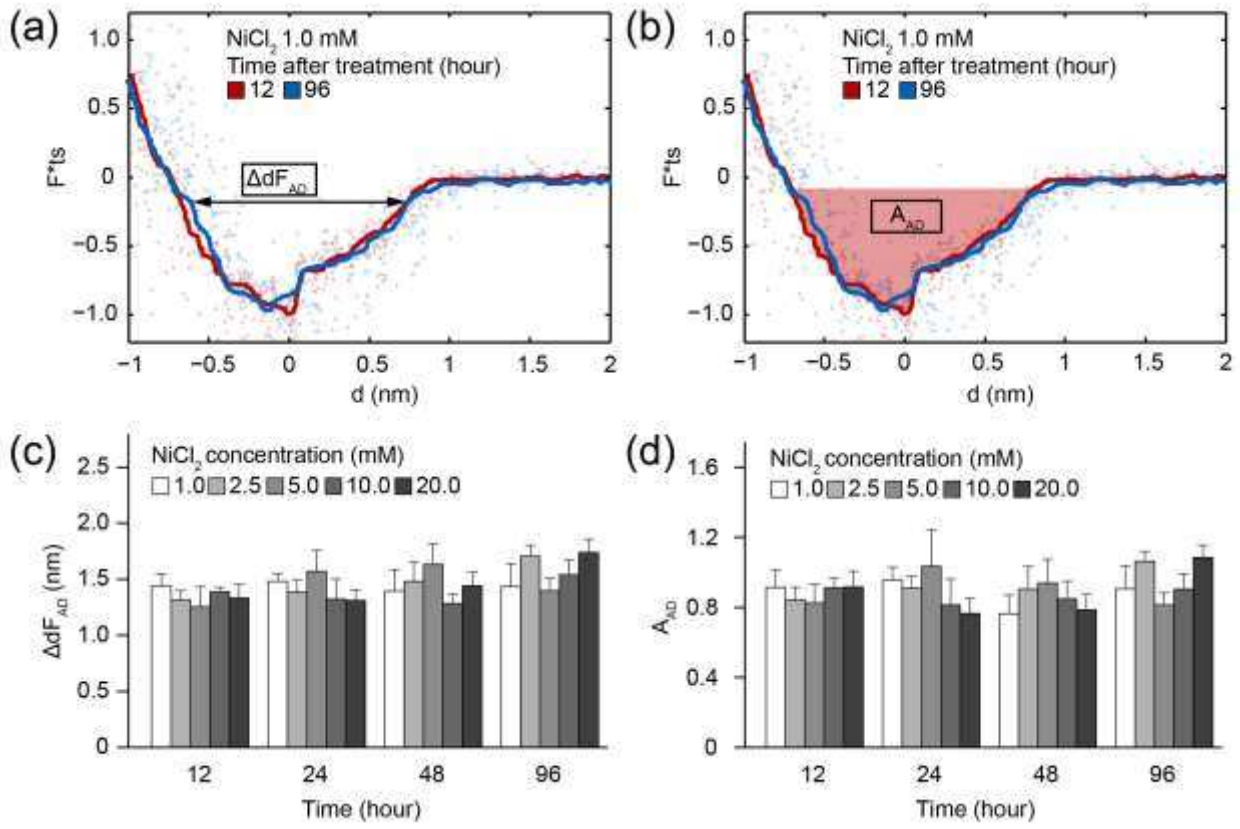

Figure 4: Normalized force profiles of mica surface incubated with 1.0 mM $NiCl_2$ solution for 5 minutes versus d. (a) shows the ΔdF_{AD} and (b) shows the A_{AD} at 12 hours (red) and 96 hours (blue) after ions treatment. Comparable values (c) ΔdF_{AD} (d) A_{AD} are observed at different time points. Each bar represents 15 force curves taken at different regions of the surface.

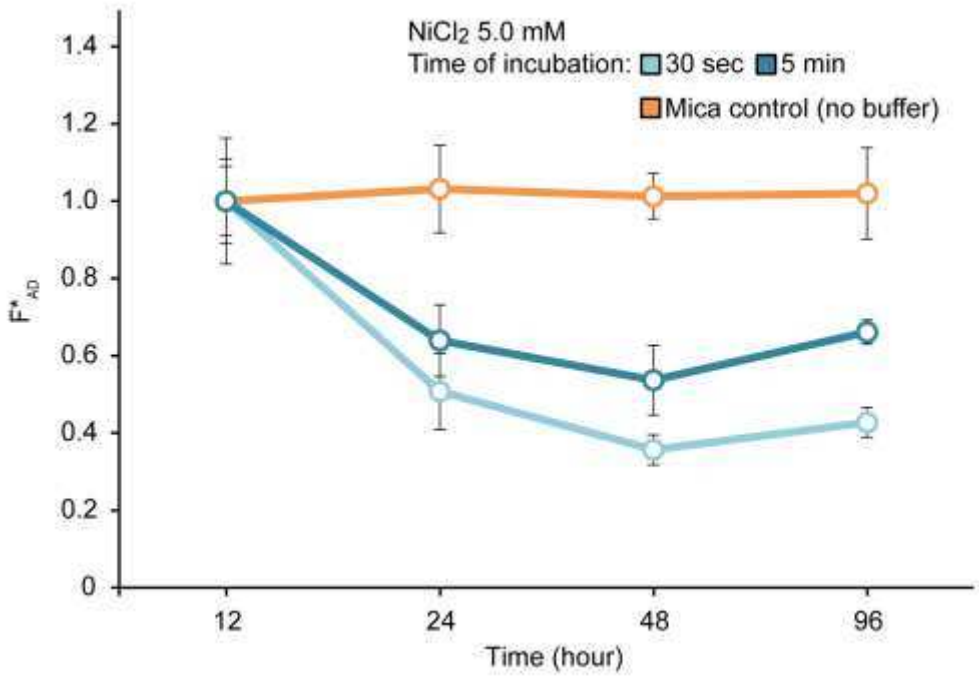

Figure 5: Evolution in time of the normalized force of adhesion of mica treated with 5.0 mM $NiCl_2$ solution for 30 seconds and 5 minutes as compared with a mica control, not treated with $NiCl_2$.

CONCLUSION

The accumulation of water on muscovite mica surfaces ion-exchanged with nickel ions has been probed at the nanoscale by a combination of atomic force microscopy techniques using silicon tips, where the physico-chemical state of those tips is carefully monitored. Non-contact imaging of the surfaces in combination with double-stranded DNA as height calibration markers (molecular dip-sticks) allows the water layer thickness to be determined. Amplitude-distance measurements in the dynamic mode allow direct detection of the water layer by avoidance of the cantilever bi-stability and reconstruction of the force profile.

We have demonstrated that in addition to ion species, ion concentration, and pH of the solution[8,18,37], the time-dependent incubation and aging process of the sample also play important roles in determining the ion distribution on mica surfaces. When the sample was treated with Ni^{2+} solution for a shorter period (30 seconds), the tip-sample interaction underwent a long time-scale dependent transition related to the accumulation of water on the mica surface and possibly as a consequence of surface compositional change and spatial distribution. Meanwhile, if the sample was treated for a longer period (5 minutes), this aging effect no longer existed. The thickness of the water layer reached a maximum as thermodynamic equilibrium was met immediately after ion deposition. Note that this phenomenon is independent of the ion-exchange concentration in the range tested, implying that the affinity of the Ni ions to the available sites in the mica is sub-mM. The thickness of the water layer was confirmed by extracting the van der Waals adhesion force (F_{AD}) between the silicon tip and mica, where a decay in F_{AD} signifies increased screening of the water. Based on the force profiles of tip-sample interaction at the nanoscale, we conclude that ions attract water onto to the mica surface in a time-dependent manner, both in the incubation and aging period after sample preparation.

ACKNOWLEDGEMENTS

We thank Karim Gadelrab and Dr. Sergio Santos for the help in implementing the MATLAB code for A_{AD} calculation and the valuable discussion.

REFERENCES

1. Gray, A.; Uher, C. Journal of Materials Science **1977,** 12 (5), 959-965.

2. Hepburn, D.; Kemp, I.; Shields, A. Electrical Insulation Magazine, IEEE **2000,** 16 (5), 19-24.

3. Müller, K.; Chang, C. Surface Science **1969,** 14 (1), 39-51.

4. Gaines Jr, G. L. The Journal of Physical Chemistry **1957,** 61 (10), 1408-1413.

5. Pashley, R. M. Journal of colloid and interface science **1981,** 83 (2), 531-546.

6. Pashley, R. M.; Israelachvili, J. N. Journal of colloid and interface science **1984,** 101 (2), 511-523.

7. Pashley, R.; Quirk, J. Colloids and surfaces **1984,** 9 (1), 1-17.

8. Hsueh, C.; Chen, H.; Gimzewski, J. K.; Reed, J.; Abdel-Fattah, T. M. ACS applied materials & interfaces **2010,** 2 (11), 3249-56.

9. Amadei, C. A.; Santos, S.; Pehkonen, S. O.; Verdaguer, A.; Chiesa, M. The Journal of Physical Chemistry C **2013,** 117 (40), 20819-20825.

10. Santos, S.; Barcons, V.; Verdaguer, A.; Font, J.; Thomson, N. H.; Chiesa, M. Nanotechnology **2011,** 22 (34), 345401.

11. Santos, S.; Verdaguer, A.; Souier, T.; Thomson, N., H.; Chiesa, M. Nanotechnology **2011,** 22 (46), 465705.

12. Kasas, S.; Thomson, N. H.; Smith, B. L.; Hansma, P. K.; Miklossy, J.; Hansma, H. G. International Journal of Imaging Systems and Technology **1997,** 8 (2), 151-161.

13. Thomson, N. H. In Applied Scanning Probe Methods, Vol VI: Characterization, Bhushan, B.; Fuchs, H.; Hosaka, S., Eds. Springer-Verlag: Berlin, 2006.

14. Pastré, D.; Hamon, L.; Landousy, F.; Sorel, I.; David, M.-O.; Zozime, A.; Le Cam, E.; Piétrement, O. Langmuir : the ACS journal of surfaces and colloids **2006,** 22 (15), 6651-6660.

15. Pastre, D.; Pietrement, O.; Fusil, S.; Landousy, F.; Jeusset, J.; David, M. O.; Hamon, L.; Le Cam, E.; Zozime, A. Biophysical journal **2003,** 85 (4), 2507-18.

16. Rivetti, C.; Guthold, M.; Bustamante, C. Journal of molecular biology **1996,** 264 (5), 919-932.

17. Hansma, H. G. Annual review of physical chemistry **2001,** 52 (1), 71-92.

18. Hansma, H. G.; Laney, D. E. Biophysical journal **1996,** 70 (4), 1933-1939.

19. Bustamante, C.; Vesenka, J.; Tang, C. L.; Rees, W.; Guthold, M.; Keller, R. Biochemistry **1992,** 31 (1), 22-26.

20. Sader, J. E.; Jarvis, S. P. Applied Physics Letters **2004,** 84 (10), 1801-1803.

21. Katan, A. J.; Van Es, M. H.; Oosterkamp, T. H. Nanotechnology **2009,** 20 (16), 165703.

22. Amadei, C. A.; Tang, T. C.; Chiesa, M.; Santos, S. The Journal of Chemical Physics **2013,** 139 (8), 084708-7.

23. Amadei, C. A.; Santos, S.; Pehkonen, S.; Verdaguer, A.; Chiesa, M. Journal of Physical Chemistry C **2013,** In print.

24. Balmer, T. E.; Christenson, H. K.; Spencer, N. D.; Heuberger, M. Langmuir : the ACS journal of surfaces and colloids **2008,** 24 (4), 1566-9.

25. Rodriguez, T. R.; Garcia, R. Applied Physics Letters **2002,** 80 (9), 1646-1648.

26. García, R.; San Paulo, A. Physical Review B **1999,** 60 (7), 4961-4967.

27. Garcia, R.; San Paulo, A. Ultramicroscopy **2000,** 82 (1-4), 79-83.

28. Santos, S.; Guang, L.; Souier, T.; Gadelrab, K.; Chiesa, M.; Thomson, N. H. Review of Scientific Instruments **2012,** 83 (4), 043707-11.

29. Guzman, H. V.; Perrino, A. P.; Garcia, R. ACS nano **2013,** 7 (4), 3198-3204.

30. Santos, S.; Stefancich, M.; Hernandez, H.; Chiesa, M.; Thomson, N. H. The Journal of Physical Chemistry C **2012,** 116 (4), 2807-2818.

31. Verdaguer, A.; Santos, S.; Sauthier, G.; Segura, J. J.; Chiesa, M.; Fraxedas, J. Physical chemistry chemical physics : PCCP **2012,** 14 (46), 16080-7.

32. Sergio, S.; Albert, V.; Tewfic, S.; Neil, H. T.; Matteo, C. Nanotechnology **2011,** 22 (46), 465705.

33. Santos, S.; Barcons, V.; Christenson, H. K.; Billingsley, D. J.; Bonass, W. A.; Font, J.; Thomson, N. H. Applied Physics Letters **2013,** 103 (6), 063702.

34. Rybenkov, V. V.; Cozzarelli, N. R.; Vologodskii, A. V. Proceedings of the National Academy of Sciences **1993,** 90 (11), 5307-5311.

35. Bates, A. D.; Maxwell, A. DNA topology. Oxford university press: 2005.

36. Santos, S.; Barcons, V.; Christenson, H. K.; Font, J.; Thomson, N. H. PloS one **2011,** 6 (8), e23821.

37. Ellis, J. S.; Abdelhady, H. G.; Allen, S.; Davies, M. C.; Roberts, C. J.; Tendler, S. J.; Williams, P. M. Journal of microscopy **2004,** 215 (Pt 3), 297-301.